Optics Communications 466 (2020) 125636

Contents lists available at ScienceDirect

Optics Communications

journal homepage: www.elsevier.com/locate/optcom

High-precision time transfer over a local ring fiber link

Rongrong Xu [a], Faxing Zuo [a], Liang Hu [a], Jianping Chen [a,b], Guiling Wu [a,b,*]

[a] Shanghai Institute for Advanced Communication and Data Science, State Key Laboratory of Advanced Optical Communication Systems and Networks, Department of Electronic Engineering, Shanghai Jiao Tong University, Shanghai 200240, China

[b] Shanghai Key Laboratory of Navigation and Location-Based Services, Shanghai 200240, China

ARTICLE INFO

Keywords:
Time transfer via optical fiber
Distributed time transfer
Ring fiber link

ABSTRACT

We propose a low-cost scheme for multi-access time transfer with high-precision over a local ring fiber link. The time signals are delivered to both the clockwise and anticlockwise directions over a single optical fiber by employing the same wavelengths. The proposed scheme is validated in experiment over a fiber–optic loop link with different lengths. The results demonstrate that the time deviation (TDEV) of less than 20 ps/s and 2 ps/10^4 s can be achieved for the fiber link up to 70 km. The evaluated uncertainty is less than 354 ps, which is mainly limited by the employed time interval counters. The maximum number of accommodated nodes is also theoretically evaluated based on the conditions of signal attenuation and backscattering effect.

1. Introduction

Precise time transfer has been recognized as one of the most important technologies in long-haul applications such as satellite navigation, deep space networks and very long baseline interferometry (VLBI) [1,2]. For some application scenarios under local environment, high precision time transfer with multiple nodes is also required. For example, in large ground-based and sea-based phased array radars, time information between multiple channels is essential, which is related to the imaging quality of the radar [3]. For large-scale cosmic ray observation experiments, in order to correlate the arrival time of the shower particles at each detection point, all time measurement nodes are required to have synchronized reference clocks, while the distributed clock synchronization systems need to distribute clock and absolute time information to clock nodes that are several kilometers apart [4]. Low cost and simple structure are also important considerations for local area applications. Traditional satellite-based time transfer technologies [5,6], for instance, global positioning system (GPS), satellite two-way time comparison and so on, are significantly affected by the free space environment, resulting in the limited accuracy. Meanwhile, they are also facing the challenges of complex system, high cost, low security and reliability. Furthermore, time transfer based on coaxial cables is subject to its bandwidth and high loss, limiting its transfer distance within 1km. With the development of optical communications over the last decades, optical fiber can be accessible all over the world. On account of the advantages of large bandwidth, low loss and strong anti-interference, the effectiveness and reliability of fiber–optic time transfer to achieve high-precision transfer have been demonstrated [7–12]. Aiming at satisfying the requirement of the applications with multiple users, point-to-multipoint optical fiber time transfer schemes with various topologies have been proposed and demonstrated [13–15]. However, none of the above schemes are specifically designed for local application environments which need not only low cost and complexity but also high precision. White Rabbit (WR) technique is a performing and cost-effective time transfer scheme in local areas [13], however, the accuracy of WR is limited by the bidirectional asymmetry of link propagation delays for using a single fiber with different wavelengths or two fibers for bidirectional transmission. The bidirectional propagation delay asymmetry can be calibrated [16], while the calibration has a precision limited by the employed calibration method and measurement devices, and often needs to take a time of long enough. In [14], L. Sliwczynski et al. realized multipoint time transmission over a bus-type network with active taps. Nevertheless, bidirectional transmission utilizing different wavelengths suffers from the transmission delay asymmetry as a result of the dispersion effect of the fiber, which requires a complex link calibration procedure. Z. Jiang et al. proposed a method for time transfer using a ring fiber link based on a wavelength tunable laser and a Mach–Zehnder Modulator (MZM) [15]. However, this scheme is not suitable for the local area applications due to its high cost of the laser with a large wavelength tunable range. The ring network is one of the most basic topologies in fiber–optic transmission networks, and it is a common network topology for area-oriented services [17,18]. Furthermore, it has unique protection function that can significantly improve the security and reliability of the fiber network [19,20].

In this letter, we present a high-precision time transfer scheme via a local ring fiber network, which has remarkable superiorities of

* Correspondence to: 5-200, SEIEE Bld. Shanghai Jiao Tong University, Shanghai 200240, China.
E-mail address: wuguiling@sjtu.edu.cn (G. Wu).

https://doi.org/10.1016/j.optcom.2020.125636
Received 30 September 2019; Received in revised form 1 February 2020; Accepted 27 February 2020
Available online 2 March 2020

low cost and complexity. By adopting the same transceiver for bidirectional transmission in a single fiber, the symmetry of the fiber link propagation delays along two directions are guaranteed completely. In the case, high precision time transfer can be reached for there is no limitation from bidirectional link delay asymmetry, and can be operated and maintained relatively simple and easy for without requiring extra link calibration. The multi-access mechanism is achieved by tapping the bidirectional optical signals with an assistance of passive optical splitters. In this way, the time information can be obtained at any location of the fiber–optic ring link. The proposed scheme is validated by the experiment over different fiber lengths, together with a theoretical analysis of the uncertainty. The time deviations (TDEV) of less than 20 ps/s and 2 ps/10^4 s are reached for the fiber link up to 70 km. The calculated combined uncertainty is less than 354 ps, which is mainly limited by the employed time interval counters. To evaluate the maximum extendibility of the proposed scheme, we estimate the number of accommodated nodes along the ring fiber link based on the signal attenuation and backscattering effects. The results show that as many as 185 slave nodes can be accessed along a 10 km ring fiber link, without considering the connector losses and reflections.

2. Principle

Fig. 1 illustrates the diagram of the proposed scheme. The major node and each slave node are interconnected through a fiber ring. At the major node, the 1 PPS (One Pulse Per Second) signal from the reference is encoded into a time code through an encoder and modulated onto an optical carrier. The modulated optical signal is split into two branches by an optical coupler (OC1), which is, respectively, sent both clockwise and anticlockwise into the fiber ring. Since the optical signals in both directions use the same wavelength, the symmetry of the bidirectional transmission delay of the primary fiber link is maximally guaranteed. The optical signal propagating along the clockwise path passes through the entire fiber loop and returns back to the major node. The 1 PPS signal is recovered after passing through an optic/electro (O/E) converter and decoder. The major node measures the time difference between the local input 1 PPS and the received 1 PPS, which is the total loop delay T_1. The total loop delay is sent to each slave node combined with 1 PPS signal by encoded into the time code. At an arbitrary slave node, a 2 × 2 optical directional coupler is inserted into the main fiber, which extracts some part of the optical signals transferred in both the clockwise and anticlockwise directions. The time codes are extracted by two O/E converters, and then enter the decoder. The decoder restores the 1 PPS signals coming from two directions respectively. The time difference between the two 1 PPS signals T_P is measured. The principle of time transfer over a ring fiber–optic link is shown in Fig. 2. The transmission and reception delays τ_{TMf}, τ_{RSf}, τ_{RSb} include the hardware delays of the major or the slave node and the transmission delays in the optical couplers. In addition to the hardware delays in the major node, τ_{TMb} also includes the transmission delays in the optical coupler and the circulator while τ_{RMf} includes the transmission delay in the circulator. The propagation delays of the cables are also included in the transmission and reception delays (τ_{TMf}, τ_{TMb}, τ_{RMf}, τ_{RSf}, τ_{RSb}).

Based on the delay model and Fig. 2, we have

$$\begin{cases} \Delta T_{MSf} = \tau_{TMb} + \delta_{MSb} + \tau_{RSb} - T_P \\ \Delta T_{MSf} + \delta_{SMf} - \tau_{RSf} + \tau_{RMf} = T_1 \end{cases} \tag{1}$$

where ΔT_{MSf} is the time difference between the local 1 PPS signal at the major node and the 1 PPS signal received at the slave node in the clockwise direction.

From Eq. (1), we have

$$\Delta T_{MSf} = \frac{1}{2}\left[(T_1 - T_P) + (\tau_{TMb} - \tau_{RMf} + \tau_{RSf} + \tau_{RSb}) + (\delta_{MSb} - \delta_{SMf})\right] \tag{2}$$

Similarly, the time difference between the local 1 PPS signal at the major node and the 1 PPS signal received at the slave node in the anticlockwise direction can be expressed as,

$$\Delta T_{MSb} = \frac{1}{2}\left[(T_1 + T_P) + (\tau_{TMb} - \tau_{RMf} + \tau_{RSf} + \tau_{RSb}) + (\delta_{MSb} - \delta_{SMf})\right] \tag{3}$$

Since the major node sends the time signals in both directions using the same wavelength over a single fiber link, the last terms in Eqs. (2) and (3) can be considered as zero. τ_{TMb}, τ_{RMf}, τ_{RSf}, τ_{RSb}, are only related to the electric/optical cables and electric/optical devices at both nodes. Therefore, these values can be calibrated by high-precision measurements [21].

3. Experimental results and discussions

The experimental setup of the proposed scheme is shown in Fig. 3, which contains a major node and a slave node. The whole experiment platform is located at the laboratory with an hourly temperature fluctuation of about 3 °C. At the major node, the 1 PPS signal from the rubidium clock (HJ210-BDRB) is encoded into the time code via a dedicated codec implemented in a FPGA platform [22]. Then it is modulated on an optical carrier with a wavelength of 1549.32 nm through a small form-factor pluggable (SFP) optical module (SFP1). A 1 × 2 50/50 optical coupler is used to divide the optical signal into two branches. The optical signal that returns to the major node through the entire fiber loop along the clockwise path is extracted by the optical circulator and then reaches the optical receiving port of SFP1. Afterwards, the 1 PPS signal is decoded by a decoder. The time interval between the received 1 PPS signal and the local 1 PPS at the major node is measured by the time interval counter (TIC1). At the slave node, a 2 × 2 10/90 optical coupler is adopted to tap out part of the optical signals transmitted both clockwise and anticlockwise from the fiber loop, the optical signals coming from the anticlockwise and clockwise directions are received by the SFP2 and SFP3, respectively. The output electrical signals of both directions are sent to the FPGA for decoding, recovering the clockwise and anticlockwise transmitted 1 PPS signals. The time interval counter (TIC2) measures the time interval between the two 1 PPS signals. The TIC3 is used to measure the "true" time difference ΔT_{MSf_M} between the time signal received by the slave node in the clockwise direction and the local time signal at the major node. The system performance is evaluated by comparing the time difference of ΔT_{MSf} and ΔT_{MSf_M}. All the adopted TICs in our test are 53230A (Keysight Technologies).

Although the bidirectional delay symmetry can be maximally guaranteed by adopting the single fiber link with the same wavelength for bidirectional transmission, the existence of Rayleigh backscattering will deteriorate the signal-to-noise ratio (SNR) of the receiving end and increase the time jitter of the timing signal as the increase of the fiber link length, which is the main limiting factor of the performance of the time/frequency transfer system [23]. To examine the performance impairment due to Rayleigh backscattering, we first connect the sending end and the receiving end of the major node directly with a spooled fiber with the lengths of 10 km and 70 km, with no slave node inserting into the link. A variable optical attenuator (VOA) is cascaded just behind the isolator at the clockwise transmitting end of the major node, in order to adjust the signal to backscattering optical power ratio (SBR) of the receiving end. The results show that when SBR is less than 15 dB, there will have recovered errors for the 1 PPS signal for both link lengths. To further demonstrate the performance of the time transfer at the worst case, we select the location along the fiber link in which the slave node is located at the end of the fiber loop in the clockwise direction and connected to the major node with a fiber jumper in the anticlockwise direction. By adjusting the VOA, the SBR is set at the minimum requirement of 15 dB. Under this link configuration, the SNR difference between the two receivers of the slave node is the largest,

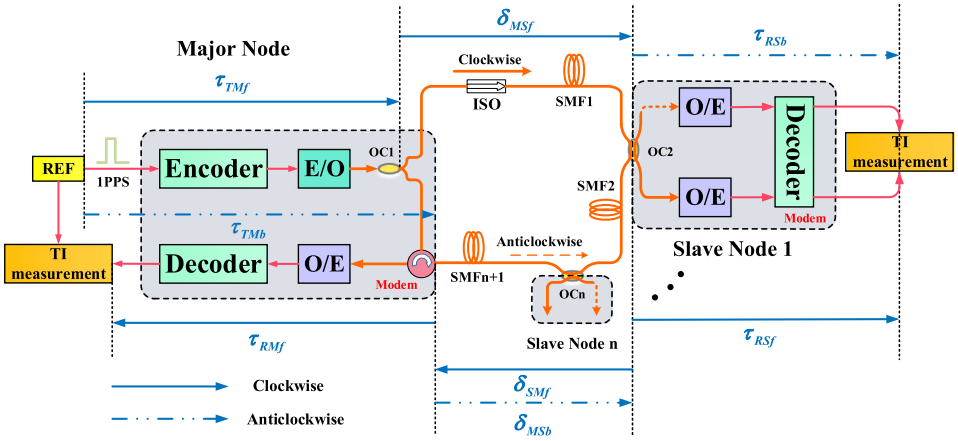

Fig. 1. Schematic of the proposed fiber–optic time transfer scheme accompany with the delay model of the scheme. REF: reference, TI: time interval, OC: optical coupler, ISO: optical isolator, SMF: single-mode fiber. τ_{TMf}, τ_{TMb} are the transmission delays of the major node in both the clockwise (forward) and anticlockwise (backward) directions. τ_{RMf} is the reception delay of the major node in the clockwise direction. τ_{RSf}, τ_{RSb} are the reception delays of the slave node in both directions. δ_{MSf}, δ_{SMf}, δ_{MSb} are the one-way propagation delays of the fiber.

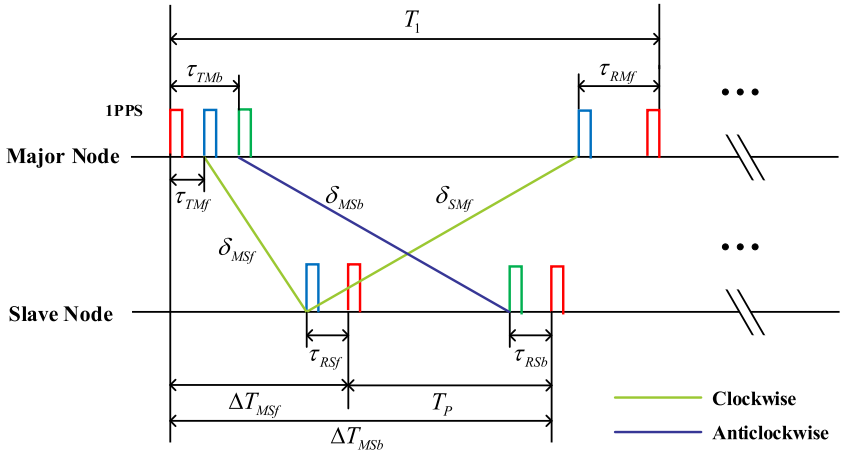

Fig. 2. The principle of time transfer over a ring fiber–optic network.

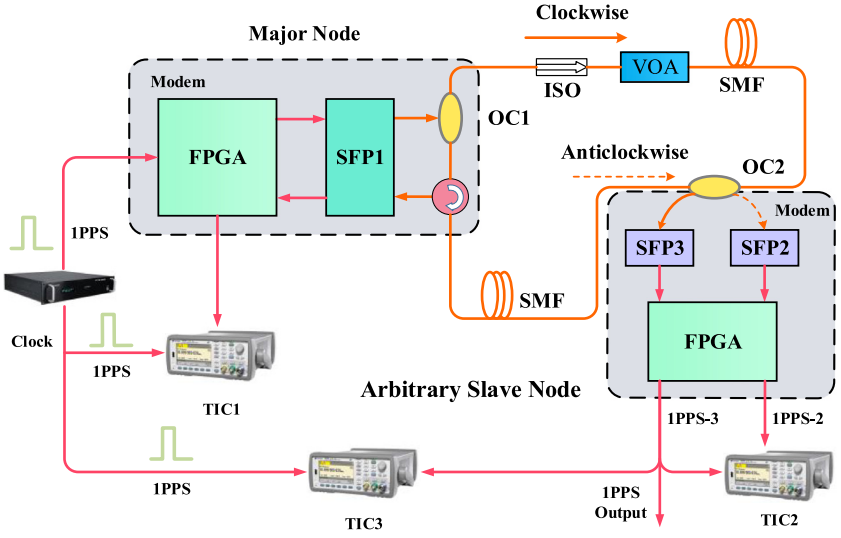

Fig. 3. Experimental setup of the proposed time transfer over a ring fiber–optic link. FPGA: Field Programmable Gate Array, SFP: small form-factor pluggable, VOA: variable optical attenuator.

and the performance of the system is the worst compared with other link configurations.

Fig. 4 shows the stabilities of the proposed time transfer scheme in terms of time deviation (TDEV) over different fiber lengths. The

Table 1
Uncertainty budget for the proposed time transfer scheme over 70 km fiber in a field implementation.

Uncertainty source	Coefficient	Estimated value	Uncertainty contribution	Uncertainty type
Time interval	1	1.16 ps	1.16 ps	A
	$\sqrt{2}/2$	250 ps	176.8 ps	B
Modem calibration	1	1.1 ps	1.1 ps	A
	$\sqrt{6}/2$	250 ps	306.2 ps	B
Wavelength difference	$0.5DL$	0 pm	0 ps	B
PMD	$0.5\sqrt{L}$	0.05 ps/$\sqrt{\text{km}}$	0.2 ps	B
Sagnac effect	$2\omega/c^2$[a]	δA_E[b]	0.2 ps	B
Combined standard uncertainty			353.6 ps	A&B

[a] ω is the rotation angular speed of the Earth, c is the speed of light in vacuum.
[b] A_E is the equatorial projection area of the surface swept by the vector from the center of the Earth and moving along the fiber, δ is the relative accuracy, it can be assumed as 10^{-3} when the accuracy of positioning fiber path on the earth is better than 1 km [8].

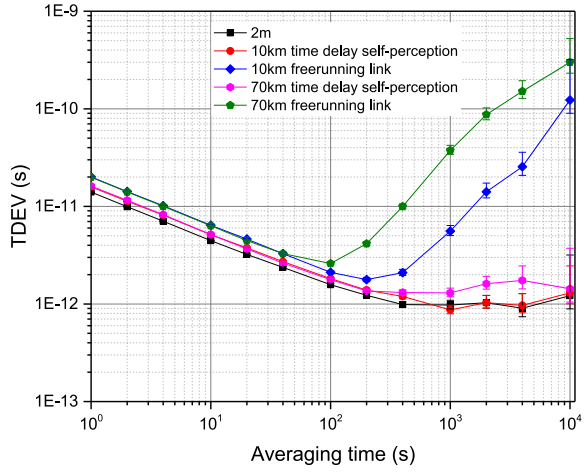

Fig. 4. The TDEV of time transfer over different fiber lengths compared with the stability of the time delay between the major node and the slave node in the clockwise direction for free running. The error bars show the 0.683 confidence range.

stability of the time delay between the major node and the slave node in the clockwise direction for free running of 10 km and 70 km spooled fiber links are also included in it. For free running link, the fluctuation of propagation delay is on the order of nanoseconds. Through the proposed scheme, the time delay between the major and the slave node at the slave node can be accurately perceived. We evaluate the performance of the proposed scheme by comparing the time difference between the measured and deduced time offset. It should be clear that the long-term stability (100–10^4 s) is significantly improved compared with the free running. The TDEV of time transfer over 2 m fiber link, less than 14.5 ps/s and 1.3 ps/10^4 s respectively, shows the floor of our experimental system in the test conditions. The floor is mainly limited by the codecs, SFP transceivers and the TICs used. The stabilities of the 10 km link are less than 17 ps/s and 2 ps/10^4 s. When the fiber length is extended to 70 km, the short term stability less than 20 ps/s has no obvious difference, while long stability slightly deteriorates. The deterioration of long-term stability is mainly due to the fluctuation of transmitting and receiving time delays at each node, which is mainly caused by environment temperature fluctuations. It should be noted that the stability almost does not degrade when the fiber length is extended to 10 km and 70 km, which indicates that the performance of the system is close to and limited by the floor.

In order to remove the effect of $\left(\tau_{TMb}-\tau_{RMf}+\tau_{RSf}+\tau_{RSb}\right)/2$ in Eq. (2), which are related to the electric/optical cables and electric/optical devices at the major node and the slave node, a modem calibration is performed for each slave node. In the modem calibration, the major node and the slave node are connected by two short fibers to form a small ring just as in Fig. 3. The measurement values of the three TICs, $\Delta T^0_{MSf\_M}$, T^0_1 and T^0_P, are obtained. Considering $\left(\delta_{MSb}-\delta_{SMf}\right)/2$ is zero for short fibers, the modem calibration value is obtained according to Eq. (2),

$$\frac{1}{2}\left(\tau_{TMb}-\tau_{RMf}+\tau_{RSf}+\tau_{RSb}\right)=\Delta T^0_{MSf\_M}-\frac{1}{2}\left(T^0_1-T^0_p\right) \tag{4}$$

The components of uncertainty budget for the proposed time transfer scheme over 70 km fiber are summarized in Table 1 and analyzed as follows. The first term includes the uncertainty in determining the time intervals (T_1, T_P) in Eq. (2). We see $\left(T_1-T_P\right)/2$ as a whole to evaluate an overall type A uncertainty. It is calculated on 200 observations [24]. The result is 1.16 ps. The uncertainty of 53230A used is about 250 ps when considering its linearity and offset (the systematic part of the uncertainty is mainly considered, the random part is negligible since this part can be reduced to a very low value by averaging, the timebase part can also be neglected since we employ the same timebase for all TICs.) [25]. According to Eq. (2), the coefficient should be $\sqrt{2}/2$, and the total type B uncertainty related to the two used TICs is 176.8 ps.

The second term results from the uncertainty of modem calibration for determining $\left(\tau_{TMb}-\tau_{RMf}+\tau_{RSf}+\tau_{RSb}\right)/2$ in Eq. (2). The standard deviation of the modem calibration value is 15 ps, which is determined with the 53230As for 200 measured data points. The corresponding type A uncertainty is 1.1 ps. The uncertainty of measurements caused by TICs can be considered as a type B uncertainty. Based on previous analysis in the first term, the uncertainty for each employed 53230A is 250 ps. According to Eq. (4), the coefficient should be $\sqrt{6}/2$ and the contributions of three TICs to the type B uncertainty of measurements are 306.2 ps.

The third to the fifth terms are originating from the fiber link, i.e. $\left(\delta_{MSb}-\delta_{SMf}\right)/2$ in Eq. (2). The bidirectional delay difference of the same fiber mainly comes from the wavelength-difference dependent fiber chromatic dispersion, polarization mode dispersion (PMD), and the Sagnac effect, and can be expressed as

$$\left(\delta_{MSb}-\delta_{SMf}\right)/2=\frac{1}{2}DL\left(\lambda_b-\lambda_f\right)+\tau_{PMD}+\tau_{sagnac} \tag{5}$$

where λ_b and λ_f are the wavelengths for the anticlockwise and clockwise directions, D is the fiber dispersion coefficient, L is the length of the fiber, τ_{PMD} is the random PMD term, τ_{sagnac} is the term from the Sagnac effect.

Since the optical signals in both directions come from the same SFP transceiver, the wavelengths are the same and the wavelength difference is zero. The uncertainty from the influence of PMD can be evaluated using the coefficient of 0.05 ps/$\sqrt{\text{km}}$ [26]. The Sagnac effect can be calculated using the coefficient of $2\omega/c^2$, which is below 1 ps for a 70 km long fiber link [8,26].

According to the above analyses, the calculated combined standard uncertainty budget is 353.6 ps for 70 km fiber–optic time transfer, which is dominated by the uncertainty related to the time interval measurement (250 ps for each 53230A) in the first and second terms. Advanced time interval measurement devices can be employed to significantly improve the uncertainty of system [8,27].

Table 2 summarizes the time difference between the measured and deduced time offset ($\Delta T_{MSf}-\Delta T_{MSf\_M}$) over different fiber lengths

Table 2
The time difference between the measured and deduced time offset over different fiber lengths after modem calibration.

Link length	Time difference	Theoretical uncertainty
2 m	0 ps	±353.6 ps
10 km	9.8 ps	±353.6 ps
70 km	−9.1 ps	±353.6 ps

without any fiber link calibration. The transmission and reception delays of two nodes, $\left(\tau_{TMb} - \tau_{RMf} + \tau_{RSf} + \tau_{RSb}\right)/2$, is calibrated by modem calibration. It can be seen that the time differences between the measured and deduced time offset are consistent with the calculated uncertainty. It is worth explaining that the calculated uncertainty mainly comes from the adopted TICs, not from our system itself.

To further evaluate the scalability of the proposed scheme, we estimate the number of accommodated nodes along the ring fiber link based on the signal attenuation and backscattering effects (for simplicity, the attenuation and reflection of connectors are not taken into consideration.). The noise resulting from self-beating of Rayleigh backscattering light and beating with the received signal is the dominant noise at each receiving end. According to our experimental measurement, when the SBR of the receiving end is greater than 15 dB, 1 PPS signal error will not occur, that is, the receiver can obtain the time information correctly and the system can work normally. Therefore, the limiting factors for capacity analysis are the SBR and the receiving sensitivity at each receiving end. The capacity analysis problem can be summarized as the following maximization problem, i.e. [28,29],

$$\begin{aligned}
\text{maximize} \quad & N \\
\text{subject to} \quad & P_{RF0} - P_{sen} > 0; \\
& 10\log 10\left(P_{RF0}\right) - 10\log 10\left(P_{FSRB0}\right) > 15; \\
& P_{RFi} - P_{sen} > 0; \qquad i = 1, \ldots, N \\
& P_{RBi} - P_{sen} > 0; \qquad i = 1, \ldots, N \\
& 10\log 10\left(P_{RFi}\right) - 10\log 10\left(P_{FSRBi}\right) > 15; \qquad i = 1, \ldots, N \\
& 10\log 10\left(P_{RBi}\right) - 10\log 10\left(P_{BSRBi}\right) > 15; \qquad i = 1, \ldots, N
\end{aligned} \tag{6}$$

where N is the number of the slave nodes in the fiber link, P_{RF0} is the desired signal of the major node in the clockwise direction, P_{FSRB0} is the single Rayleigh backscattering (SRB) received at the major node, $P_{RFi}(i = 1, \ldots, N)$ and $P_{RBi}(i = 1, \ldots, N)$ are the desired signals of each slave node in both the clockwise and anticlockwise directions, $P_{FSRBi}(i = 1, \ldots, N)$ and $P_{BSRBi}(i = 1, \ldots, N)$ are the SRB received at each slave node in both the clockwise and anticlockwise directions.

For the calculations, the transmitting optical power in either direction of the major node $P_{in} = -1$ dBm, the Rayleigh backscattering coefficient $R_B = -33$ dB, the receiving sensitivity at each receiving end $P_{sen} = -30$ dBm. Assuming all slave nodes are distributed uniformly along the ring fiber link and the coupling ratio of optical coupler at each slave node is identical, the number of accommodated nodes over different fiber link lengths (10 km, 30 km, 50 km and 70 km) with different coupling ratios of optical couplers are estimated and plotted in Fig. 5. We can clearly see that an optimal coupling ratio for the maximum number of accommodated slave nodes can be found for each fiber link length. For instance, the maximum number of slave nodes that can be accommodated in a 10 km optical fiber link is 185, while only 14 can be accommodated in a 70 km link. This can be explained that for too low coupling ratios, the optical power obtained from the receiving end of some slave nodes is lower than the receiving sensitivity, and the corresponding electrical signal cannot be demodulated by the receiving end. When the coupling ratio is too large, the number of the accommodatable slave nodes of the link is limited by SBR at the receiving end of the major node. The higher the coupling ratio is, the smaller the optical signal power can be received by the major node along the main ring fiber link. The results indicate that the proposed scheme is more suitable for local short-haul networks. Although similar time transfer stability can be obtained over long distances, the number of nodes that can be accommodated is low.

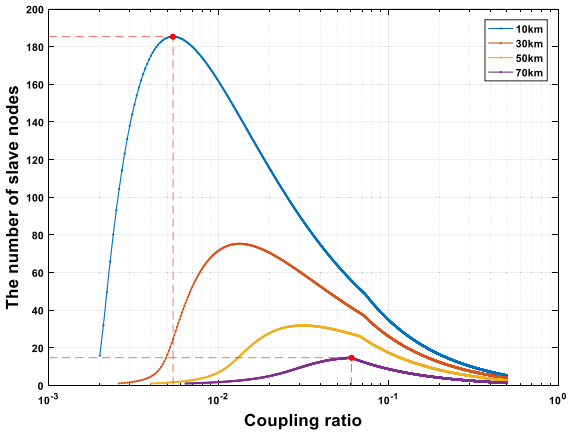

Fig. 5. The number of slave nodes vs. the coupling ratio over different-length fiber links.

4. Conclusion

In summary, we proposed and experimentally demonstrated a high-precision fiber–optic time transfer scheme based on a ring topology. The multi-access mechanism is achieved by adopting optical transceiver modules and passive optical splitters, which is a lower cost technique for the application with multiple users. Moreover, the main limiting factor of the system performance deriving from Rayleigh backscattering is experimentally evaluated. The system can work without 1 PPS signal errors when the SBR of each receiving end is more than 15 dB. The time transfer performance of the proposed scheme is also demonstrated over 10 km and 70 km fiber loop links under the minimum SBR of 15 dB. Different factors related to the uncertainty of time transfer are investigated in detail by theoretical analyses and full uncertainty budget for the system is calculated. The results illustrate that the uncertainty of less than 354 ps and the stabilities of less than 20 ps/s and 2 ps/10^4 s can be achieved at the intermediate points. According to the limitation of signal attenuation and the influence of the Rayleigh backscattering, the maximum number of slave nodes over different lengths of fiber link with different coupling ratios and is theoretically analyzed.

CRediT authorship contribution statement

Rongrong Xu: Investigation, Visualization, Writing - original draft. **Faxing Zuo:** Software, Data curation. **Liang Hu:** Methodology, Writing - review & editing. **Jianping Chen:** Supervision. **Guiling Wu:** Conceptualization, Writing - review & editing, Funding acquisition.

Acknowledgment

This work was supported by the National Natural Science Foundation of China (NSFC) (61627817, 61905143), and science and technology project of State Grid Corporation of China (SGSHJX00KXJS1901531).

References

[1] D. Calonico, C. Clivati, M. Frittelli, A. Mura, M. Zucco, F. Levi, F. Perini, C. Bortolotti, M. Roma, R. Ambrosini, G.A. Costanzo, Time and frequency optical fiber links for space metrology, in: 2015 2nd IEEE International Workshop on Metrology for Aerospace (Metroaerospace), 2015, pp. 204–208.

[2] D.S. Robertson, Geophysical applications of very-long-baseline interferometry, Rev. Modern Phys. 63 (1991) 899–918.

[3] S.-Q. Hu, F. Liu, T. Long, Design and realization of phased array radar optical fiber transmission system, J. Beijing Inst. Technol. 16 (2007) 87–92.

[4] Q. Du, G. Gong, W. Pan, A packet-based precise timing and synchronous DAQ network for the LHAASO project, Nucl. Instrum. Methods Phys. Res. 732 (2013) 488–492.

[5] D. Piester, A. Bauch, L. Breakiron, D. Matsakis, B. Blanzano, O. Koudelka, Time transfer with nanosecond accuracy for the realization of international atomic time, Metrologia 45 (2008) 185–198.

[6] J. Levine, A review of time and frequency transfer methods, Metrologia 45 (2008) S162.

[7] M. Rost, D. Piester, W. Yang, T. Feldmann, T. Wubbena, A. Bauch, Time transfer through optical fibres over a distance of 73 km with an uncertainty below 100 ps, Metrologia 49 (2012) 772–778.

[8] Ł. Śliwczyński, P. Krehlik, A. Czubla, Ł. Buczek, M. Lipiński, Dissemination of time and RF frequency via a stabilized fibre optic link over a distance of 420 km, Metrologia 50 (2013) 133–145.

[9] H. Zhang, G.L. Wu, L. Hu, X.W. Li, J.P. Chen, High-precision time transfer over 2000-km fiber link, IEEE Photonics J. 7 (2015).

[10] J. Vojtěch, O. Havliš, M. Šlapák, P. Škoda, V. Smotlacha, R. Velc, P. Münster, J. Kundrát, M. Altmann, J. Radil, Joint stable optical frequency and precise time transfer over 406 km of shared fiber lines—Study, in: 2017 40th International Conference on Telecommunications and Signal Processing (TSP), IEEE, 2017, pp. 694–697.

[11] P. Jansweijer, H. Peek, E. De Wolf, White rabbit: Sub-nanosecond timing over ethernet, Nucl. Instrum. Methods Phys. Res. A 725 (2013) 187–190.

[12] N. Kaur, P. Tuckey, P.E. Pottie, Time transfer over a white rabbit network, in: 2016 European Frequency and Time Forum (EFTF), IEEE, 2016, pp. 1–4.

[13] M. Lipinski, T. Wlostowski, J. Serrano, P. Alvarez, White rabbit: a PTP application for robust sub-nanosecond synchronization, in: International IEEE Symposium on Precision Clock Synchronization for Measurement Control & Communication, 2011.

[14] L. Sliwczynski, P. Krehlik, Multipoint joint time and frequency dissemination in delay-stabilized fiber optic links, IEEE Trans. Ultrason. Ferroelectr. Freq. Control 62 (2015) 412–420.

[15] Z.Z. Jiang, Y.T. Dai, A.X. Zhang, F.F. Yin, J.Q. Li, K. Xu, Q. Lv, T.P. Ren, G.S. Tang, Precise time delay sensing and stable frequency dissemination on arbitrary intermediate point along fiber-optic loop link with RF phase locking assistance, IEEE Photonics J. 7 (2015).

[16] G. Daniluk, White rabbit calibration procedure version 1.0, in: CERN BE-CO-HT, 2014, available at: http://www.ohwr.org/documents/2132014.

[17] A. Qasim, T. Mehmood, U. Ali, Q.U. Khan, S. Ghafoor, Dual-ring radio over fiber system with centralized light sources and local oscillator for millimeter-wave transmission, 2018.

[18] V. Kamchevska, Y. Ding, M.S. Berger, L. Dittmann, M. Galili, The Hi-Ring Architecture for Data Center Networks, 2018.

[19] K. Gou, C. Gan, X. Zhang, Y. Zhang, A tangent-ring optical TWDM-MAN enabling three-level transregional reconfigurations and shared protections by multipoint distributed control, Opt. Commun. 410 (2018) 855–862.

[20] X.F. Li, C.Q. Gan, Y.J. Chen, H.B. Qiao, Y.Q. Yan, Dual-fiber-ring architecture supporting discretionary peer-to-peer intra-communication and bidirectional inter-communication in metro-access network, IEEE Access 7 (2019) 52360–52370.

[21] D. Matsakis, F. Arias, A. Bauch, J. Davis, T. Gotoh, M. Hosokawa, D. Piester, On Optimizing the Configuration of Time-Transfer Links Used to Generate TAI, Frequency & Time Forum, 2006.

[22] G.L. Wu, L. Hu, H. Zhang, J.P. Chen, High-precision two-way optic-fiber time transfer using an improved time code, Rev. Sci. Instrum. 85 (2014).

[23] Ł. Śliwczyński, P. Krehlik, M. Lipiński, Optical fibers in time and frequency transfer, Meas. Sci. Technol. 21 (2010) 075302.

[24] J. JCGM, Evaluation of measurement data—Guide to the expression of uncertainty in measurement, Int. Organ. Stand. Geneva ISBN 50 (2008) 134.

[25] Agilent 53230A Series RF/Universal Frequency Counter/Timersx, Data Sheet, Agilent Technologies, Inc., USA, 2010.

[26] P. Krehlik, L. Sliwczynski, L. Buczek, M. Lipinski, Fiber-optic joint time and frequency transfer with active stabilization of the propagation delay, 61 (2012) 2844–2851.

[27] P. Krehlik, J. Kołodziej, H. Schnatz, D. Piester, A. Bauch, H. Imlau, H. Ender, Calibrated optical time transfer of UTC (k) for supervision of telecom networks, Metrologia 56 (2018) 015006.

[28] L. Sliwczynski, J. Kolodziej, Bidirectional optical amplification in long-distance two-way fiber-optic time and frequency transfer systems, IEEE Trans. Instrum. Meas. 62 (2013) 253–262.

[29] M.S. Bazaraa, H.D. Sherali, C.M. Shetty, Nonlinear Programming: Theory and Algorithms, John Wiley & Sons, 2013.